# Forced Waves in a Baroclinic Shear Flow. Part 2: Damped and Undamped Response to Weak Near-Resonant Forcing

R. ALAN PLUMB

*CSIRO, Division of Atmospheric Physics, Aspendale, 3195, Australia*

(Manuscript received 17 December 1980, in final form 27 April 1981)

ABSTRACT

This paper is a continuation of a study of the response of a two-layer baroclinic fluid to weak, near-resonant planetary wave forcing. Unlike Part I (Plumb, 1979), the fluid is baroclinically stable and viscous damping is incorporated into the model. With no damping, periodic solutions are found which are similar to but simpler than those of Part 1. With the addition of damping, multiple steady solutions are possible, in agreement with results of earlier studies, notably Charney and DeVore (1979). The importance of nonlinear resonance, the relationships between inviscid and viscous dynamics, and the time scales on which these processes act are investigated by numerical integration of a series of initial value problems.

## 1. Introduction

In Part I of this study (Plumb, 1979) the properties of forced waves in a weakly stable baroclinic shear were discussed. The inviscid analysis assumed weak forcing at a phase velocity close to the two free wave speeds of the system. Under certain conditions the steady solution predicted by linear theory was found to be unstable as a result of interaction with the two free modes; this behavior led to temporary amplification of the wave response and a concomitant depletion of the baroclinic shear. Solutions were shown to be periodic in time, but it was recognized that neglect of dissipative processes might be a serious shortcoming in this regard.

Similar behavior has been found in severely truncated models of barotropic planetary waves by Charney and DeVore (1979), Paegle (1979) and Fischer (1980). Despite the dynamical differences between these models and that of Part 1, the governing equations and stability criteria of the two approaches are in most respects analogous. Charney and DeVore solved the damped barotropic problem and found the possibility of multiple steady solutions. In some cases stable steady solutions of both "high-index" (weak wave, strong zonal flow) and "low-index" (strong wave, weak zonal flow) types were found to exist for the same external parameters. The latter, which Charney and DeVore identified with atmospheric blocking patterns, were associated with a nonlinear resonance phenomenon in which the mean state is locked in a quasi-resonant configuration. Similar results were obtained by Davey (1980). Both Charney and DeVore (1979) and Davey confirmed that these results are not crucially dependent on the model truncation by comparison with results from numerical models of higher resolution. Hart (1979) and Trevisan and Buzzi (1980) also found the same behavior in models with weak forcing by highly anisotropic topography without any *a priori* truncation. Hart discussed in detail the bifurcation and hysteresis associated with the existence of multiple stable solutions in some regions of parameter space. Recently, Charney and Straus (1980) have performed a similar analysis in a baroclinic two-layer system. While the evolutionary properties are similar, the energetics are quite different from those of the barotropic case.

In this paper the analysis of Part 1 is extended to include dissipation. This could not be done close to the baroclinic instability threshold (as in Part 1) since dissipation destabilizes the basic state in this region (Romea, 1977) and it was thought desirable to avoid such instabilities in order to circumvent possible ambiguities in the results. Therefore, the basic state is taken to be baroclinically stable to a finite degree at the wavelength of interest. Viscosity is incorporated via Ekman layer friction on the top and bottom bounding surfaces which move in opposite directions with constant zonal velocity. A planetary wave is introduced into the model by specifying a weak wave forcing at the lower boundary. As in Part 1 the regime of interest—that in which nonlinear interaction can take place within the time scale on which dispersion occurs between forcing and response—is such that the phase velocity of the forcing is close to one of the free wave speeds. No *a priori* truncation is necessary—under these assumptions generation of higher order wave modes is negligible at the order of interest.

0022-4928/81/091856-14$07.50

Evolution equations for the wave response and the wave-induced mean flow correction are derived. Their properties, steady states and stability characteristics are investigated with and without damping; results correspond with those obtained in Part 1 and in previous studies on the topic. Particular attention is paid to the transient behavior of solutions evolving from given initial conditions.

## 2. The evolution equations

The system to be considered is basically that of Pedlosky (1970) which was modified in Part 1 to allow wave forcing at the lower boundary of a two-layer fluid. The fluid is confined in a channel beta plane with rigid sidewalls on $y = 0, 1$ and, in the vertical, by a horizontal rigid surface at $z = D$. A wave is introduced by specifying on the lower boundary ($z = 0$) a vertical velocity

$$W = \tfrac{1}{2}\,\mathrm{Re}\, ik\delta^{3/2}\epsilon e^{ik(x-ct)} \sin m\pi y, \qquad (2.1)$$

where $\delta \ll 1$ and $\epsilon$ (which is of order unity) may be a slowly varying function of time. Note that this formulation, to leading order, incorporates the possibility of the forcing arising from topography, since then $W = U_2 \partial h/\partial x$, where $U_2$ is the zonal velocity of the lower layer. With topographic forcing, however, there are higher order corrections to be made to $W$, corresponding to interaction of the topography with the wave field itself. Unlike Part 1, these corrections are not unimportant at the order of interest in this problem. However, they do not influence the form of the final evolution equation for the wave response; this point will be discussed further below.

The Rossby number Ro and Ekman number E are assumed small. Then the governing equations for the streamfunctions $\psi_n$ in the upper and lower layers respectively are (the notation is that of Part 1)

$$\left.\begin{aligned}
&\left(\frac{\partial}{\partial t} + \frac{\partial \psi_1}{\partial x}\frac{\partial}{\partial y} - \frac{\partial \psi_1}{\partial y}\frac{\partial}{\partial x}\right) \\
&\qquad \times (\nabla^2 \psi_1 + \mathrm{F}(\psi_2 - \psi_1) + \beta y) \\
&\qquad\qquad = \frac{-\mathrm{E}^{1/2}}{\mathrm{Ro}} \nabla^2 \psi_1 \\
&\left(\frac{\partial}{\partial t} + \frac{\partial \psi_2}{\partial x}\frac{\partial}{\partial y} - \frac{\partial \psi_2}{\partial y}\frac{\partial}{\partial x}\right) \\
&\qquad \times (\nabla^2 \psi_2 + \mathrm{F}(\psi_1 - \psi_2) + \beta y) \\
&\qquad\qquad = -2W - \frac{\mathrm{E}^{1/2}}{\mathrm{Ro}} \nabla^2 \psi_2
\end{aligned}\right\}, \qquad (2.2)$$

where F is the internal rotational Froude number (Pedlosky 1970).

Now the regime of interest is that for which the basic state is stable to baroclinic waves, i.e., if the basic-state zonal velocities in the two layers are $U_1 = -U_2 = U$, then $2U$ is smaller than the critical shear for baroclinic instability $U_c = 2\beta \mathrm{F}/[\kappa^2(4\mathrm{F}^2 - \kappa^4)^{1/2}]$ (where $\kappa$ is the total wavenumber of the wave of interest) by a finite amount. For the given wavenumber the free wave phase velocities are, in the inviscid limit, the two solutions of

$$c_0 = \frac{-\beta(\kappa^2 + \mathrm{F})}{\kappa^2(\kappa^2 + 2\,\mathrm{F})} \pm \frac{[\kappa^4(\kappa^4 - 4\,\mathrm{F}^2)U^2 + \beta^2\,\mathrm{F}^2]^{1/2}}{\kappa^2(\kappa^2 + 2\,\mathrm{F})}. \qquad (2.3)$$

In the interests of tractability attention is restricted to small amplitude forcing $\delta \ll 1$. Therefore, nonlinear interactions are weak unless the phase speed of the forcing is sufficiently close to one of the free wave speeds (2.3). The reason for this is that the evolution of the forced wave is, as noted in Part 1, crucially dependent on the interaction between the forced stationary wave and free-traveling wave modes. The time scale for dispersion between one of the free waves and the forcing is $T_{\mathrm{disp}} \propto (c - c_0)^{-1}$. Now, the forced wave amplitude is proportional to $W(c - c_0)^{-1}$ and therefore the induced mean flow correction is proportional to $W^2(c - c_0)^{-2}$. Hence the time scale for nonlinear interaction is proportional to $(c - c_0)^2/W^2$, which is comparable with $T_{\mathrm{disp}}$ when $(c - c_0)^3 \sim W^2$, i.e., $c - c_0 \sim \mathrm{O}(\delta)$. Detuning on this time scale is accommodated by specifying $c = c_0$ in (2.1) but allowing $\epsilon = \epsilon(T)$, where

$$T = \delta t \qquad (2.4)$$

is the long nonlinear time scale. Dissipation also is assumed to act on this time scale (otherwise it would dominate the nonlinearity), so we write

$$\frac{\mathrm{E}^{1/2}}{\mathrm{Ro}} = \delta R, \qquad (2.5)$$

where $R \lesssim \mathrm{O}(1)$.

Solutions to (2.2) are sought in the form

$$\psi_n = -U_n y + \delta^{1/2}\phi_n^{(1)} + \delta\phi_n^{(2)} + \delta^{3/2}\phi_n^{(3)} + \delta^2\phi_n^{(4)} \cdots, \qquad (2.6)$$

where $\phi_n^{(j)} = \phi_n^{(j)}(x, y, t, T)$. We also expand $W = \delta^{3/2}W^{(3)} + \cdots$. At $\mathrm{O}(\delta^{1/2})$, the solution comprises linear wave solutions, *viz.*,

$$\left.\begin{aligned}
\phi_1^{(1)} &= \mathrm{Re} A(T) e^{ik(x-c_0t)} \sin m\pi y \\
\phi_2^{(1)} &= \mathrm{Re}\gamma A(T) e^{ik(x-c_0t)} \sin m\pi y
\end{aligned}\right\}, \qquad (2.7)$$

where

$$\gamma = \frac{\kappa^2 + \mathrm{F}}{\mathrm{F}} - \frac{(\beta + 2\,\mathrm{F}U)}{\mathrm{F}(U - c_0)}. \qquad (2.8)$$

Of course, the solutions (2.7) are valid for any $(k, m)$; however, attention here is restricted to cases where the leading order response has the same wavenum-

ber as the forcing. This is strictly valid *provided* there are no pairs of free modes in the system that can form a resonant triad with the forced wave. For a zonally bounded system, there may be a countably infinite set of values of the forcing phase velocity for which resonant triads may occur. For the purposes of this analysis, it is assumed that $c$ does not coincide with one of these values and therefore we identify $(k, m)$ in (2.7) with the wavenumbers of the forcing (2.1).

At O($\delta$), Eq. (2.2) gives two identical equations for the wave components of $\phi_n^{(2)}$, *viz.*,

$$\frac{\partial}{\partial x}(\phi_2^{(2)} - \gamma\phi_1^{(2)}) = 0. \tag{2.9}$$

Pedlosky (1970) noted that there is no point in adding more wavelike terms of the form (2.7) at this order since no phase shift is introduced.[1] Therefore, without loss of generality, the solution at this order is a mean flow correction

$$\phi_n^{(2)} = \Phi_n^{(2)}(y, T) \tag{2.10}$$

yet to be determined.

At O($\delta^{3/2}$), Eqs. (2.2) give

$$\left(\frac{\partial}{\partial t} + U\frac{\partial}{\partial x}\right)[\nabla^2\phi_1^{(3)} + \mathrm{F}(\phi_2^{(3)} - \phi_1^{(3)})] + (\beta + 2\,\mathrm{F}U)\frac{\partial\phi_1^{(3)}}{\partial x} = -\mathrm{Re}\left\{\left(\frac{\partial}{\partial T} - ik\frac{\partial\Phi_1^{(2)}}{\partial y}\right)[\gamma\,\mathrm{F} - (\mathrm{F} + \kappa^2)]\right.$$
$$\left. + ik\frac{\partial}{\partial y}\left[\frac{\partial^2\Phi_1^{(2)}}{\partial y^2} + \mathrm{F}(\Phi_2^{(2)} - \Phi_1^{(2)})\right] - \kappa^2 R\right\} Ae^{ik(x-c_0t)}\sin m\pi y, \tag{2.11a}$$

$$\left(\frac{\partial}{\partial t} - U\frac{\partial}{\partial x}\right)[\nabla^2\phi_2^{(3)} + \mathrm{F}(\phi_1^{(3)} - \phi_2^{(3)})] + (\beta - 2\,\mathrm{F}U)\frac{\partial\phi_2^{(3)}}{\partial x} = -\mathrm{Re}\left\{\left(\frac{\partial}{\partial T} - ik\frac{\partial\Phi_2^{(2)}}{\partial y}\right)[\mathrm{F} - \gamma(\mathrm{F} + \kappa^2)]\right.$$
$$\left. + ik\gamma\frac{\partial}{\partial y}\left[\frac{\partial^2\Phi_2^{(2)}}{\partial y^2} + \mathrm{F}(\Phi_1^{(2)} - \Phi_2^{(2)})\right] - \gamma\kappa^2 R\right\} Ae^{ik(x-c_0t)}\sin m\pi y - 2W^{(3)}. \tag{2.11b}$$

Note from (2.1) that

$$2W^{(3)} = \mathrm{Re}\,ik\epsilon(T)e^{ik(x-c_0t)}\sin m\pi y. \tag{2.12}$$

The low-order solutions are revealed by suppression of secularities in the higher order equations, thus ensuring the validity in time of the expansion (2.6). This is achieved by requiring that the projection of the forcing term in the simultaneous equations (2.11) on the solution of the homogeneous equations vanish. This process is straightforward, the result being

$$\frac{1}{ik}\left[\frac{(U + c_0)}{(U - c_0)}(\beta + 2\,\mathrm{F}U) + \gamma^2\frac{(U - c_0)}{(U + c_0)}(\beta - 2\,\mathrm{F}U)\right]\frac{dA}{dT} + A\left[\frac{\kappa^2 R}{ik}\left[(U + c_0) - \gamma^2(U - c_0)\right]\right.$$
$$+ 2\int_0^1 \left\{\left[\gamma^2\frac{(U - c_0)}{(U + c_0)}(\beta - 2\,\mathrm{F}U)\Phi_2^{(2)} + \frac{(U + c_0)}{(U - c_0)}(\beta + 2\,\mathrm{F}U)\Phi_1^{(2)}\right]\right.$$
$$+ (U + c_0)\left[\left(\frac{\partial^2}{\partial y^2} - \mathrm{F}\right)\Phi_1^{(2)} + \mathrm{F}\Phi_2^{(2)}\right] - \gamma^2(U - c_0)\left[\left(\frac{\partial^2}{\partial y^2} - \mathrm{F}\right)\Phi_2^{(2)} + \mathrm{F}\Phi_1^{(2)}\right]\Big\}$$
$$\left.\times \sin 2m\pi y dy\right] = -\gamma(U - c_0)\epsilon. \tag{2.13}$$

Solution of Eqs. (2.11) for $\phi_n^{(3)}$ comprises, in general, the sum of a wave term and a mean flow correction; the latter turns out to be unimportant at the order of interest. For the wave term we are free to demand, without loss of generality, that all the wave structure in the upper layer is described by the leading order term $\phi_1^{(3)}$; the phase shift introduced by $\phi_2^{(3)}$ cannot, however, be neglected and therefore $\phi_n^{(3)}$ is written

$$\left.\begin{aligned}\phi_1^{(3)} &= 0\\ \phi_2^{(3)} &= \mathrm{Re}\,d_2 e^{ik(x-c_0t)}\sin m\pi y\end{aligned}\right\}, \tag{2.14}$$

where, from (2.11a),

$$ik\,\mathrm{F}(U - c_0)d_2 = -[\mathrm{F}\gamma - (\mathrm{F} + \kappa^2)]\frac{dA}{dT}$$
$$+ A\left[\kappa^2 R + 2ik\int_0^1 \frac{\partial}{\partial y}\left\{[\gamma\,\mathrm{F} - (\mathrm{F} + \kappa^2)]\Phi_1^{(2)}\right.\right.$$
$$\left.\left. - \left(\frac{\partial^2}{\partial y^2} - \mathrm{F}\right)\Phi_1^{(2)} - \mathrm{F}\Phi_2^{(2)}\right\}\sin^2 m\pi y dy\right]. \tag{2.15}$$

Only the zonal means of (2.2) turn out to be im-

[1] Because of the slower evolution in this case, the phase shift introduced into (2.17) of Part 1 by the transience of the O($\delta^{1/2}$) solution does not arise here.

portant at $O(\delta^2)$. These are (the overbar denoting zonal average)

$$\frac{\partial}{\partial t}\left[\overline{\frac{\partial^2\phi_1^{(4)}}{\partial y^2} + F(\phi_2^{(4)} - \phi_1^{(4)})}\right] + \frac{\partial}{\partial T}\left[\frac{\partial^2\Phi_1^{(2)}}{\partial y^2} + F(\Phi_2^{(2)} - \Phi_1^{(2)})\right] + \frac{1}{2}km\pi\, F(\sin 2m\pi y)\,\mathrm{Re}(iAd_2^*) = -R\frac{\partial^2\Phi_1^{(2)}}{\partial y^2}, \quad (2.16a)$$

$$\frac{\partial}{\partial t}\left[\overline{\frac{\partial^2\phi_2^{(4)}}{\partial y^2} + F(\phi_1^{(4)} - \phi_2^{(4)})}\right] + \frac{\partial}{\partial T}\left[\frac{\partial^2\Phi_2^{(2)}}{\partial y_2} + F(\Phi_1^{(2)} - \Phi_2^{(2)})\right] - \frac{1}{4}km\pi\, F(\sin 2m\pi y)\,\mathrm{Re}(iAd_2^*) - R\frac{\partial^2\Phi_2^{(2)}}{\partial y^2} - \bar{W}^{(4)}. \quad (2.16b)$$

For the purposes of this presentation, it will be assumed that $\bar{W}^{(4)} = 0$, i.e, we set the Eulerian mean to zero and thus the forcing corresponds to the "source-sink" forcing of some laboratory experiments. This is not of course the correct relation for topographic forcing, for which the *Lagrangian* vertical velocity is zero at the lower boundary. In some related problems without sidewall boundaries this difference can have a profound influence on the leading order behavior (McEwan *et al.*, 1980). In this example, however, both approaches lead to identical evolution equations, although the definition of the coefficients differs. For example, Plumb (1981) considers an analogous (undamped) problem of topographic forcing of a continuous baroclinic shear, arriving at an evolution equation indentical in form with that to be derived here (in the inviscid limit). This being the case we here set $\bar{W}^{(4)} = 0$ since this leads to a simpler problem for which the wave-mean flow interaction is purely baroclinic in the sense that

$$\Phi_1^{(2)} = -\Phi_2^{(2)} \quad (2.17)$$

in Eqs. (2.16).

Now, from (2.15),

$$kF(U - c_0)\,\mathrm{Re}(iAd_2^*) = -\frac{1}{2}[F\gamma - (F + \kappa^2)]\frac{d|A|^2}{dT} + \kappa^2 R|A|^2 \quad (2.18)$$

and therefore the secular forcing terms in (2.16) are suppressed if

$$\frac{\partial}{\partial T}\left[\frac{\partial^2\Phi_1^{(2)}}{\partial y^2} - 2F\Phi_1^{(2)}\right] + R\frac{\partial^2\Phi_1^{(2)}}{\partial y} = \frac{m\pi}{4(U - c_0)}\left[\frac{(\beta + 2FU)}{(U - c_0)}\frac{d|A|^2}{dT} + 2\kappa^2 R|A|^2\right], \quad (2.19)$$

where (2.8), (2.17) and (2.18) have been used. The wave evolution equation (2.13) now becomes

$$\left[\frac{(U + c_0)}{(U - c_0)}(\beta + 2FU) + \gamma^2\frac{(U - c_0)}{(U + c_0)}(\beta - 2FU)\right]\frac{dA}{dT} + A\left[\kappa^2 R\{(U + c_0) - \gamma^2(U - c_0)\} + 2ik\int_0^1\left\{\left(\frac{U + c_0}{U - c_0}\right)(\beta + 2FU) - \gamma^2\left(\frac{U - c_0}{U + c_0}\right)(\beta - 2FU)\right\}\Phi_1^{(2)} + [(U + c_0) + \gamma^2(U - c_0)]\left(\frac{\partial^2}{\partial y^2} - 2F\right)\Phi_1^{(2)}\sin 2m\pi y\, dy\right] = -ik\gamma(U - c_0)\epsilon. \quad (2.20)$$

Eqs. (2.19) and (2.20) may be simplified by defining the coefficients

$$\left.\begin{aligned} a_1 &= \kappa^2[(U + c_0) - \gamma^2(U - c_0)]X^{-1} \\ b_2 &= \left[\left(\frac{U + c_0}{U - c_0}\right)(\beta + 2FU) - \gamma^2\left(\frac{U - c_0}{U + c_0}\right)(\beta - 2FU)\right]X^{-1} \\ b_3 &= [(U + c_0) + \gamma^2(U - c_0)]X^{-1} \\ a_4 &= \frac{2\kappa^2(U - c_0)}{(\beta + 2FU)} \end{aligned}\right\}, \quad (2.21)$$

and

$$\Lambda = -\gamma(U - c_0)\epsilon X^{-1},$$

where

$$X = \left(\frac{U + c_0}{U - c_0}\right)(\beta + 2FU) + \gamma^2\left(\frac{U - c_0}{U + c_0}\right)(\beta - 2FU),$$

when the evolution equations become

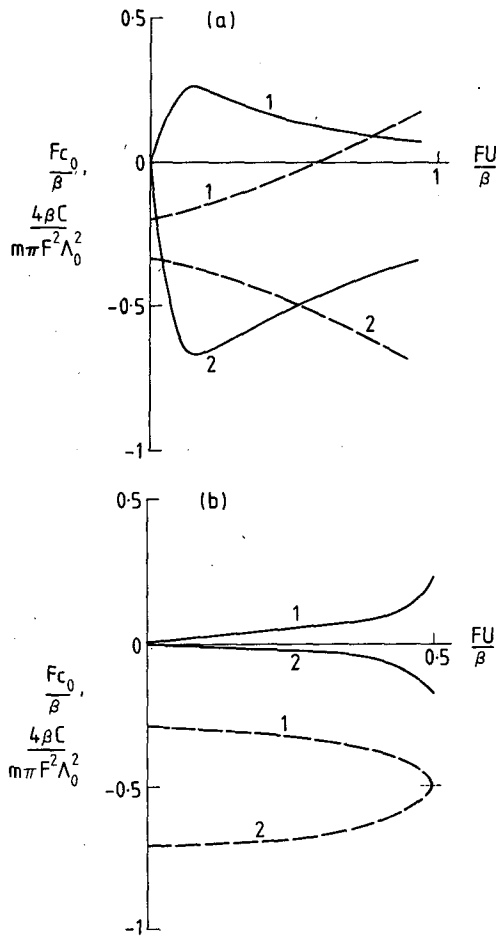


FIG. 1. Dependence of phase speed $c_0$ (dashed curve) and interaction parameter $C$ (solid curve) on the shear $U$. (a) $\kappa^2 = 3$ F, and (b) $\kappa^2 = \sqrt{2}$ F. Labels 1 and 2 identify the two wave modes.

$$\frac{dA}{dT} + a_1RA + 2ikA \times \int_0^1 \left[ b_2\Phi_1^{(2)} + b_3\left(\frac{\partial^2}{\partial y^2} - 2\,\mathrm{F}\right)\Phi_1^{(2)} \right] \times \sin 2m\pi y\,dy = ik\Lambda, \quad (2.22)$$

$$\frac{\partial}{\partial T}\left(\frac{\partial^2\Phi_1^{(2)}}{\partial y} - 2\,\mathrm{F}\Phi_1^{(2)}\right) + R\,\frac{\partial^2\Phi_1^{(2)}}{\partial y^2} = \frac{m\pi(\beta + 2\,\mathrm{F}U)}{4(U - c_0)^2}\left(\frac{d|A|^2}{dT} + a_4R|A|^2\right) \times \sin 2m\pi y. \quad (2.23)$$

Finally, we scale $A$ by the forcing amplitude and shift, on the long time scale, to a frame of reference in which the forcing is stationary; i.e., if

$$\Lambda = \Lambda_0 e^{-ik\sigma T}, \quad (2.24)$$

where $\Lambda_0$ and $\sigma$ are real, we write

$$\left.\begin{aligned} \tau &= kT \\ B &= \Lambda_0^{-1}Ae^{i\sigma\tau} \end{aligned}\right\}. \quad (2.25)$$

Further defining

$$\chi = \frac{4(U - c_0)^2}{m^2(\beta + 2\,\mathrm{F}U)}\,\frac{\Phi_1^{(2)}}{\Lambda_0^2}, \quad (2.26)$$

$$\left.\begin{aligned} a_2 &= \frac{m\pi(\beta + 2\,\mathrm{F}U)}{4(U - c_0)^2}\,\Lambda_0^2 b_2 \\ a_3 &= \frac{m\pi(\beta + 2\,\mathrm{F}U)}{4(U - c_0)^2}\,\Lambda_0^2 b_3 \end{aligned}\right\}. \quad (2.27)$$

Eqs. (2.22) and (2.23) become

$$\frac{dB}{d\tau} = i\sigma B - a_1rB - 2iB \times \int_0^1 \left[ a_2\chi + a_3\left(\frac{\partial^2}{\partial y^2} - 2\,\mathrm{F}\right)\chi \right] \times \sin 2m\pi y\,dy + i, \quad (2.28)$$

$$\frac{\partial}{\partial\tau}\left(\frac{\partial^2\chi}{\partial y^2} - 2\,\mathrm{F}\chi\right) + \frac{r\partial^2\chi}{\partial y^2} = \left(\frac{d|B|^2}{d\tau} + a_4r|B|^2\right)\sin 2m\pi y, \quad (2.29)$$

respectively, where $r = R/k$.

## 3. Inviscid solutions

If $r = 0$, Eq. (2.29) integrates to

$$\frac{\partial^2\chi}{\partial y^2} - 2\,\mathrm{F}\chi = (|B(\tau)|^2 - |B(0)|^2)\sin 2m\pi y \quad (3.1)$$

if it is assumed that the initial mean flow correction is zero, i.e.,

$$\Phi(y, 0) = 0. \quad (3.2)$$

The appropriate boundary condition for the mean flow is (e.g., Pedlosky, 1970)

$$\frac{\partial^2\Phi}{\partial y\partial t} = 0 = \frac{\partial^2\chi}{\partial y\partial\tau} \quad (3.3)$$

on $y = 0, 1$. The solution to (3.1) is then

$$\chi = \frac{-1}{2(\mathrm{F} + 2m^2\pi^2)} \times \left[\sin 2m\pi y - \frac{m\pi}{\sqrt{\tfrac{1}{2}\,\mathrm{F}}}\,\frac{\sinh\sqrt{2\,\mathrm{F}}(y - \tfrac{1}{2})}{\cosh\sqrt{\tfrac{1}{2}\,\mathrm{F}}}\right] \times [|B(\tau)|^2 - |B(0)|^2]. \quad (3.4)$$

Substituting into (2.28) gives

$$\frac{dB}{d\tau} - i\sigma B + iCB(|B|^2 - |B(0)|^2) = i, \quad (3.5)$$

where

$$C = a_3 - \frac{a_2}{2(\mathrm{F} + 2m^2\pi^2)} \times \left[1 + \frac{4m^2\pi^2}{(\mathrm{F} + 2m^2\pi^2)} \frac{\tanh\sqrt{\tfrac{1}{2}\,\mathrm{F}}}{\sqrt{\tfrac{1}{2}\,\mathrm{F}}}\right]. \quad (3.6)$$

Note from (2.27) that $C \propto \Lambda_0^2$.

Eq. (3.5) differs from that obtained in Part 1 [and a similar equation derived in similar circumstances by Fischer (1980) and by Pedlosky (1970) for the nonlinear baroclinic instability problem] in the absence of a second-order time derivative. Physically, this arises because only one free mode lies (in frequency) within the bandwidth of the nonlinear interaction, as compared with two in Part 1. Nevertheless, Eq. (4.4) of Part 1 reduces to the form (3.5) in the slow evolution limit, where one wave mode is much closer to resonance than the other and it is therefore not surprising that the properties of (3.5) turn out to be similar to those discussed in Part 1.

This is most clearly seen in the stability problem. Eq. (3.5) has a steady solution

$$B_L = -1/\sigma \quad (3.7)$$

—exactly that which would be obtained for the linear problem. As in Part 1, the stability problem for perturbations to this state give

$$\left.\begin{aligned} \mathrm{Re}(B) &= -\sigma^{-1} + \mathrm{Re}(b_R e^{s\tau}) \\ \mathrm{Im}(B) &= \mathrm{Re}(b_I e^{s\tau}) \end{aligned}\right\}, \quad (3.8)$$

where $b_R$ and $b_I$ are constants and

$$s^2 = -\sigma^2\left(1 - 2\,\frac{C}{\sigma^3}\right). \quad (3.9)$$

Therefore, the steady solution (3.7) is unstable if

$$\frac{2C}{\sigma^3} > 1. \quad (3.10)$$

This is exactly the same criterion as derived in Part I (but note that $C$ and $\sigma$ have slightly different definitions here). Similar criteria have been derived for the *a priori* truncated problem by Charney and DeVore (1979), Paegle (1979) and Fischer (1980).

According to (3.10) the solution $B = B_L$ is unstable if $\sigma$ is sufficiently small (near-resonant forcing) and of the same sign as $C$. For given $k$, $m$, $U$ and F there are two free modes (2.3); examples of calculations of $C$ are shown in Fig. 1 for cases with $\kappa^2 > 2\,\mathrm{F}$ (baroclinic stability) and $\kappa^2 < 2\,\mathrm{F}$ (baroclinic instability at sufficiently large $U$). The corresponding instability curves for the forcing phase velocity $c$ vs $U$ are shown schematically in Fig. 2. The regions of instability are bounded by the resonance curves $c = c_0$ and $c = c_0 + k\delta\sigma_c$, where from (3.10) $\sigma_c = (2C)^{1/3}$. Results from Part 1 have been incorporated into Fig. 2 in regions near the baroclinic instability threshold.

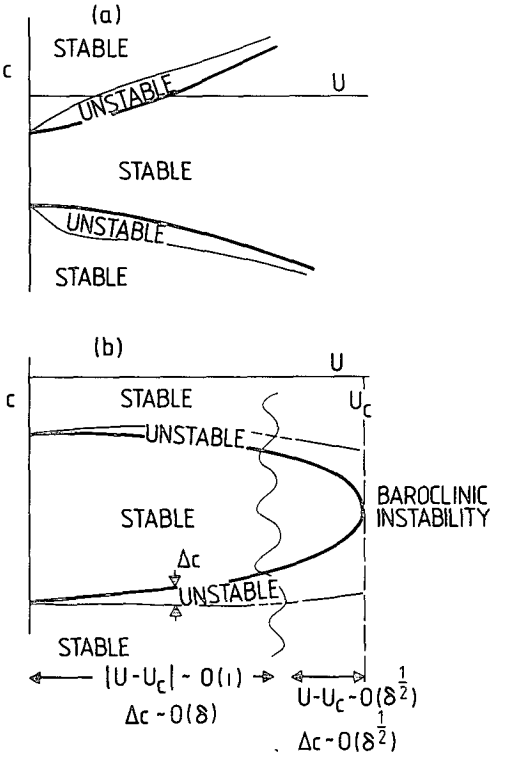


FIG. 2. Schematic diagram of the regions of instability of the linear solution $B_L$. Phase speed $c = c_0 + k\delta\sigma$ of the wave forcing plotted versus mean shear $U$. (a) $\kappa^2 > 2\,\mathrm{F}$ and (b) $\kappa^2 < 2\,\mathrm{F}$. In (b) the results of Part 1 (cf. Fig. 3 of Part 1) have been incorporated in the region $|U - U_c| \ll 1$. Heavy curves: resonance curve $c = c_0$. Light curves: nonlinear instability criterion $c = c_0 + k\delta(2C)^{1/3}$.

In Part 1 evolution of the complex wave amplitude was shown to be analogous to the motion of a particle in a rotating potential well. A similar parallel may be drawn here; with $B = X + iY$, Eq. (3.5) becomes

$$\left.\begin{aligned} \frac{dX}{d\tau} &= \frac{\partial\Phi}{\partial Y} \\ \frac{dY}{d\tau} &= -\frac{\partial\Phi}{\partial X} \end{aligned}\right\}, \quad (3.11)$$

where the "potential" $\Phi$ is

$$\Phi = \tfrac{1}{4}C(X^2 + Y^2)^2 - \tfrac{1}{2}(\sigma + C\,|B(0)|^2) \times (X^2 + Y^2) - X. \quad (3.12)$$

The properties of $\Phi$ were discussed and illustrated in Part 1. In (3.11) note that the trajectory $[X(\tau), Y(\tau)]$ in this case is exactly along the $\Phi$ contours; this corresponds with the slow evolution limit of Part 1.

Contours of $\Phi$ for the stability problem [with

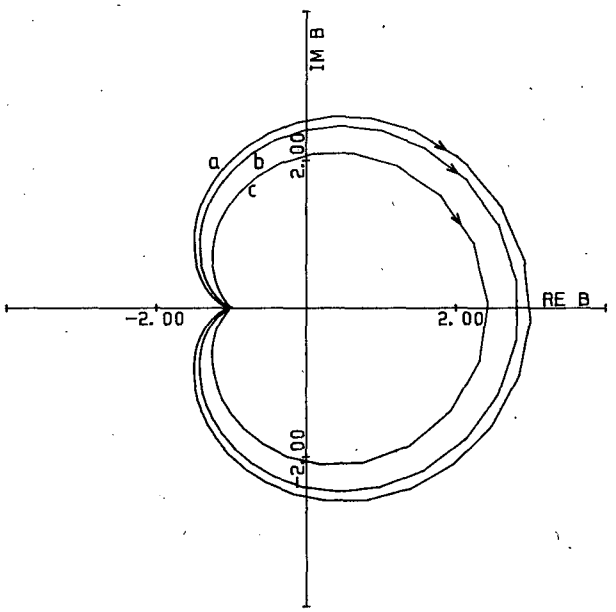


FIG. 3. Instability of steady linear solution $B_L$. Trajectories (Re$B$, Im$B$) are plotted every $\Delta\tau = 0.20$. $\sigma = 1$, $B(0) = (-1, 0.01)$. Arrow shows direction of evolution. (a) $C = 0.51$, (b) $C = 0.6$ and (c) $C = 1.0$.

$|B(0)| = 1/\sigma$] were presented in Fig. 6 of Part 1. In the stable regime, $2C/\sigma^3 < 1$, the point $B_L$ is a local minimum of $\Phi$, whereas it is a saddle point when $2C/\sigma^3 > 1$. Evolution of $B$ in the unstable regime obtained by numerical integration of (3.5) is illustrated in Fig. 3 for $\sigma = 1$ and $C = 0.51$, 0.6 and 1.0; initial conditions are $B = (1 - 0.01i)B_L$. Paegle (1979) found periodic solutions to the almost identical truncated problem in the form of elliptic functions. Fig. 3 shows the evolution to be periodic here. At first, $B$ drifts slowly away from the steady state, increasing in amplitude; subsequently evolution is more rapid as the phase of $B$ decreases. After the phase of $B$ relative to $B_L$ passes $-\pi$, the solution returns toward $B_L$ in a mirror image of its previous track. The maximum amplification $|B|/|B_L|$ attained is 3.0 for $C = 0.51$, but decreases with increasing $C$.

It was noted in Part 1 that for $1 > 2C/\sigma^3 > 0$ the linear solution $B_L$ is unstable to finite-amplitude perturbations. The same is true here, as illustrated in Fig. 4, for which $C = 0.05$, $\sigma = 1$ and with various initial conditions. Stability to small perturbations is evident for the three examples with $B(0) = (-0.5, 0)$, (0, 0) and (0.5, 0), in which cases the evolution of $B$ is an "inner" orbit of $B_L$. For large perturbations, the behavior differs significantly. With $B(0) = (1, 0)$ and (2, 0) the initial evolution is similar to the other cases but before $B$ has completed one-half of an orbit around $B_L$ the evolutionary track recurves and $B$ follows an "outer" track which is similar to that shown in the instability examples of Fig. 3. Note that this "outer" track does not enclose $B_L$.

The reasons for this behavior can best be understood by regarding $B(\tau)$ as the sum of a forced component and a free traveling wave. Note, however, that the two are coupled by the nonlinearity and therefore the latter is not strictly "free". Now, because of the transformation (2.24) the frame of reference adopted in (3.5) is one in which the forcing is stationary and the traveling wave has a resonant frequency $-\sigma$. Linear theory would then suggest that the solution, in general, would be $B(\tau) = B_L + be^{-i\omega\tau}$, where $b$ is the amplitude of the traveling wave excited by initial conditions and where $\omega = -\sigma$. We may generalize this to allow for nonlinear interaction by allowing $b = b(\tau)$, $\omega = \omega(\tau)$. The dependence of amplitude variations on phase is revealed by the wave energy equation which from (3.5) is

$$\frac{d|B|^2}{d\tau} = -2\,\mathrm{Re}(iB). \tag{3.13}$$

Therefore, when

$$0 < \arg(B) < \pi, \tag{3.14}$$

the phase relationship between the wave and the forcing is such that the wave amplitude grows; $|B|$ decreases when $\pi < \arg(B) < 2\pi$.

Qualitatively, examples a, b, c of Fig. 4—those which follow the inner orbit—behave as linear theory suggests. The orbit of $B_L$ is of course modified by nonlinear effects; $b$ and $\omega$ are not strictly constant, but their variation is not very dramatic. After $B$ has completed half an orbit, $\arg(B) > \pi$ and the

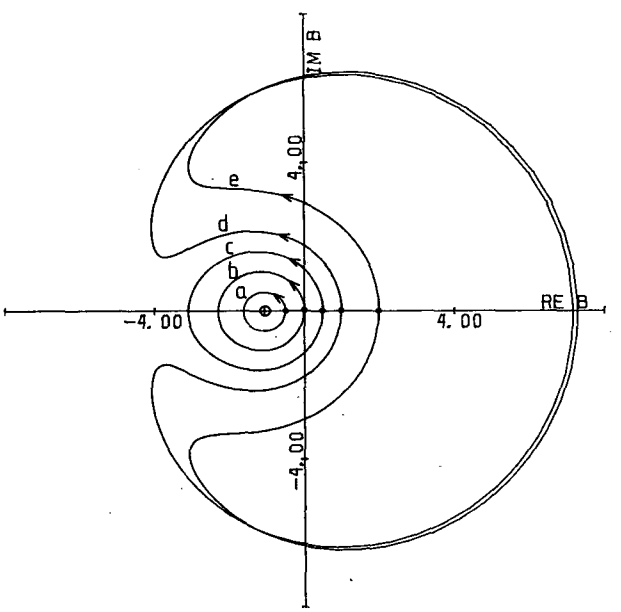


FIG. 4. Dependence of evolution of wave amplitude $B$ on initial conditions when $C/\sigma^3 > 0$. $\sigma = 1$, $C = 0.05$. Trajectories are plotted every $\Delta\tau = 0.25$. $\oplus$ denotes linear solution $B_L$; closed circles denote starting points for each run. Arrows show direction of evolution.

energy exchange with the mean flow as quantified by (3.13) changes sign; the orbit is then completed in a mirror image of the first half.

Nonlinear effects become more dramatic for large-amplitude perturbations [examples (d, e) of Fig. 4]. Initially the evolution is similar to cases (a, b, c) with $\omega \approx -\sigma$. As $|B|$ increases, however, nonlinearities reduce $\omega$ until, before arg($B$) reaches $\pi$, $\omega$ changes sign. Therefore arg($B$) declines again, maintaining the favorable relationship (3.14) for amplification until arg($B$) returns to zero. The amplification of $B$ is therefore related to a nonlinear resonance as $\omega$ is reduced to zero by nonlinear interaction; Charney and DeVore (1979) identified this phenomenon as a cause of multiple solutions in the steady damped problem.

The stability problem (3.8) may be interpreted in the same way. In this case, the free wave component is initially an infinitesimal perturbation which grows as a result of the nonlinear feedback.

When $C/\sigma^3 < 0$ nonlinear effects *increase* the free wave frequency and hence the feedback processes associated with $\omega$ changing sign do not occur. Fig. 5 shows some examples with $S = 0.05$, $\sigma = -1$; in all cases evolution takes the form of an orbit around $B_L$. Nonlinear effects are apparent only in a decrease in orbital period with increasing $|B(0) - B_L|$.

Fig. 6 shows the evolution from fixed initial conditions [$B(0) = 0$] as a function of forcing amplitude (i.e., as a function of $C$) for $\sigma = 1$. The structure of the potential $\Phi(X, Y)$ as a function of $C/\sigma^3$ was illustrated in Fig. 11 of Part 1. With these initial conditions, the bifurcation in evolution (inner vs outer track) occurs at $C/\sigma^3 = 0.0741$; this is clearly illustrated in Fig. 6. With $C \leq 0.074$, $B$ follows the inner orbit; note that nonlinear distortion of the track (which would be circular in the linear problem) is clearly evident for $C/\sigma^3 = 0.074$. Larger $C/\sigma^3$ leads to the nonlinear resonance and the consequent wave amplification; the bifurcation at $C/\sigma^3 = 0.0741$ leads to a sudden increase in the maximum value of $|B|$ by a factor of about 2. As in the instability problem (Fig. 3), $|B|_{\max}$ then decreases as $C$ increases.

Finally, note that the evolution in Fig. 6 is smoother than in the similar cases shown in Figs. 13 and 14 of Part 1. This is simply a consequence of the absence in this case of the extra, high-frequency free mode which is responsible for the rapid oscillations in the results of Part 1.

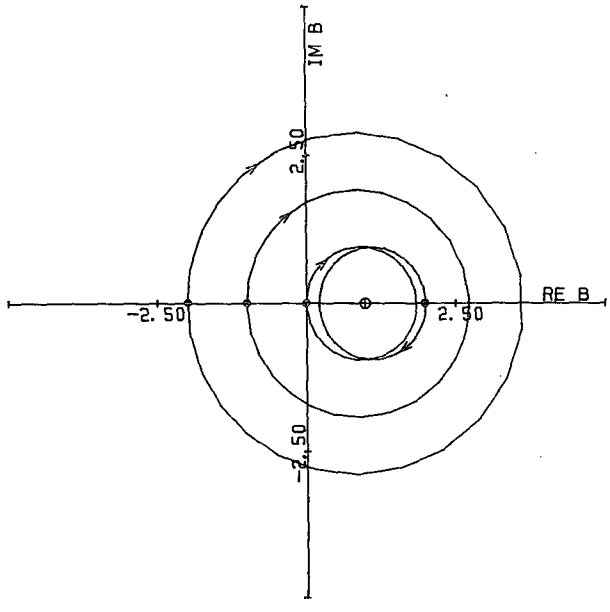


FIG. 5. Dependence of evolution of wave amplitude $B$ on initial conditions when $C/\sigma^3 < 0$. $\sigma = -1$, $C = 0.05$. Otherwise as in Fig. 4.

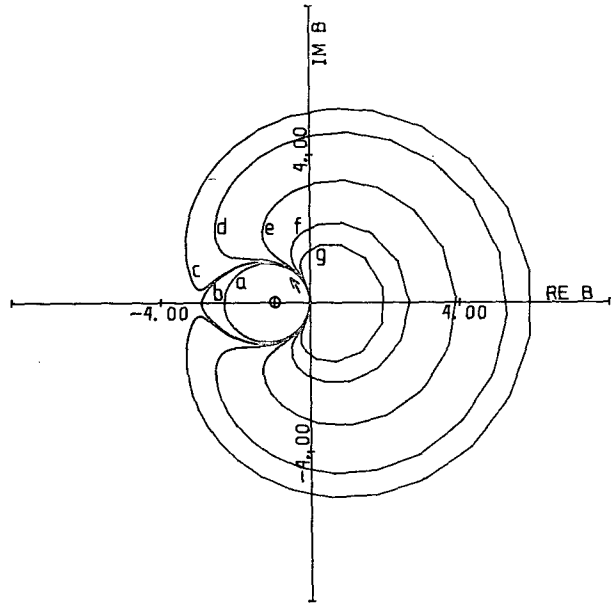


FIG. 6. Dependence of wave amplitude $B$ on forcing amplitude when $C/\sigma^3 > 0$ for $B(0) = (0, 0)$, $\sigma = 1$. Trajectories are plotted every $\Delta\tau = 0.20$. $\oplus$ denotes linear solution, arrow shows direction of evolution. (a) $C = 0.05$, (b) $C = 0.074$, (c) $C = 0.075$, (d) $C = 0.1$, (e) $C = 0.2$, (f) $C = 0.5$ and (g) $C = 1.0$.

## 4. Damped solutions, $r \neq 0$

When $r$ is nonzero the analytic solution (3.4) for the cross-channel structure of $\chi$ is inappropriate. Instead, in view of the boundary condition (3.3) we expand, following Smith (1977), to obtain

$$\chi = \sum_{n=1}^{\infty} \chi_n \cos(2n - 1)\pi y. \tag{4.1}$$

It also is necessary to expand

$$\sin 2m\pi y = \sum_{n=1}^{\infty} g_{mn} \cos(2n - 1)\pi y, \tag{4.2}$$

where

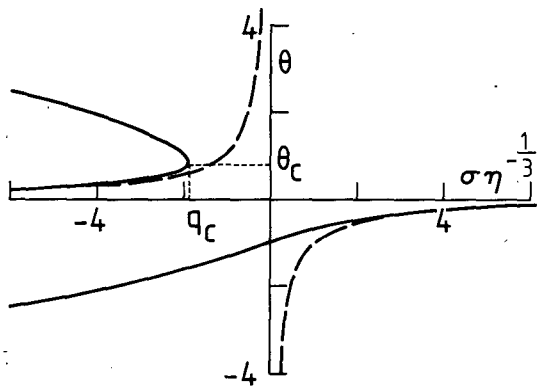


FIG. 7. Viscous steady solutions. $B_s = \eta^{-1/3}\theta$, where $\theta$ is plotted versus $\sigma\eta^{-1/3}$ (solid curve). Dashed curve: linear solution $\theta_L$. The point $(\theta_c, q_c)$ is noted in the text.

$$g_{mn} = 2\int_0^1 \sin 2m\pi y \cos(2n-1)\pi y\,dy = \frac{8m}{\pi[4m^2-(2n-1)^2]}. \quad (4.3)$$

Then (2.29) gives

$$\frac{d\chi_n}{d\tau} + \frac{r\pi^2(2n-1)^2}{[(2n-1)^2\pi^2+2\,\mathrm{F}]}\chi_n = \frac{-g_{mn}}{[(2n-1)^2\pi^2+2\,\mathrm{F}]} \times \left(\frac{d|B|^2}{d\tau} + a_4 r|B|^2\right), \quad (4.4)$$

while (2.28) becomes

$$\frac{dB}{d\tau} = (i\sigma - a_1 r)B - iB\sum_{n=1}^{\infty} g_{mn} \times \{a_2 - [2\,\mathrm{F} + \pi^2(2n-1)^2]a_3\}\chi_n + i. \quad (4.5)$$

### a. Steady solutions

The steady solution to (4.4) is $\chi_n = \chi_{ns}$, $B = B_s$, where

$$\pi^2(2n-1)^2\chi_{ns} = -g_{mn}a_4|B_s|^2. \quad (4.6)$$

Note that this balance is independent of $r$; the wave-induced forcing and viscous dissipation of the mean flow are both proportional to the Ekman number (Hart 1979). The balance (4.6) is quite different from that of the undamped problem where any steady-state satisfies (4.4) trivially. Substitution into (4.5) gives the steady solution $B = B_s$:

$$[(\sigma + ia_1 r) + \eta|B_s|^2]B_s + 1 = 0, \quad (4.7)$$

where

$$\eta = a_4\sum_{n=1}^{\infty}\frac{g_{mn}^2\{a_2 - a_3[2\,\mathrm{F} + \pi^2(2n-1)^2]\}}{\pi^2(2n-1)^2}.$$

Since

$$\sum_{n=1}^{\infty} g_{mn}^2 = 1$$

and

$$\sum_{n=1}^{\infty}\frac{g_{mn}^2}{\pi^2(2n-1)^2} = \frac{3}{4m^2\pi^2}$$

(Smith 1977),

$$\eta = a_4\left[\frac{3}{4m^2\pi^2}(a_2 - 2\,\mathrm{F}a_3) - a_3\right]. \quad (4.8)$$

Note from (2.27) that $\eta \propto \Lambda_0^2$.

Because of the different mean flow balance, $B_s$ in (4.7) differs from the inviscid solution $B_L$ even in the limit $r \to 0$, when

$$(\sigma + \eta|B_s|^2)B_s + 1 = 0. \quad (4.9)$$

For small $r$, however, the time taken to reach a steady state varies as $r^{-1}$ and therefore the inviscid solutions are valid for an increasingly longer time as $r \to 0$ (cf. Pedlosky, 1971). It is interesting to note that Trevisan and Buzzi (1980) obtained (4.9) as an equation for *inviscid* steady states; they did not make our assumption that $\chi = 0$ at $\tau = 0$.

From (4.9), $B_s$ is necessarily real as $r \to 0$, and therefore, in this limit,

$$B_s = \eta^{-1/3}\theta(\sigma\eta^{-1/3}), \quad (4.10)$$

where $\theta$ is a real solution of

$$\theta^3 + (\sigma\eta^{-1/3})\theta + 1 = 0. \quad (4.11)$$

Fig. 7 shows a plot of $\theta$, which is identical in form to Fig. 1 of Trevisan and Buzzi (1980); also plotted on Fig. 7 is the linear solution $\theta_L = -\eta^{1/3}/\sigma$. In $\sigma\eta^{-1/3} > q_c = -1.89$, there is a single steady solution, which asymptotes to $\theta_L$ as $\sigma\eta^{-1/3} \to \infty$. For $\sigma\eta^{-1/3} < q_c$, there are three steady states, only one of which asymptotes to the linear solution as $\sigma\eta^{-1/3} \to -\infty$. The other two solutions are of much larger amplitude. In the barotropic problem Charney and DeVore (1979) noted that they are characterized by a weak mean flow which is locked into a nonlinear resonance configuration; this point was explored further by Trevisan and Buzzi (1980), who noted the similarity between this problem and that of the anharmonic oscillator. Hart (1979) described the bifurcation and hysteresis implicit in Fig. 7 as $\sigma\eta^{-1/3}$ crosses $q_c$ in the positive or negative directions.

### b. Stability of the steady solution

The stability of these steady solutions has been discussed by Charney and DeVore (1979), Hart (1979) and Trevisan and Buzzi (1980). For completeness, the stability analysis is repeated here, writing

$$\left.\begin{aligned} B &= B_s + b \\ \chi_n &= \chi_{ns} + x_n \end{aligned}\right\}. \quad (4.12)$$

In the limit $r \to 0$, Eq. (4.4) gives

$$x_n = \frac{-g_{mn}}{[(2n-1)^2\pi^2 + 2\,\mathrm{F}]} B_s(b + b^*) \quad (4.13)$$

for suitable initial conditions ($x_n = 0$ when $b = 0$). Linearizing (4.5) we then find

$$\frac{db}{d\tau} - i(\sigma + \eta B_s^2)b + iCB_s^2(b + b^*) = 0. \quad (4.14)$$

This has solutions $b = \mathrm{Re}(b_R e^{st}) + i\ \mathrm{Re}(b_I e^{st})$, where

$$s^2 = (\sigma + \eta B_s^2) - [(2C - \eta)B_s^2 - \sigma]. \quad (4.15)$$

Therefore there are growing solutions if, using (4.9),

$$-2CB_s^3 > 1. \quad (4.16)$$

As a function of wave amplitude, this is exactly the same criterion as (3.10) for the inviscid problem; this is not a surprising result, in view of the inviscid dynamics in both problems (since we have taken $r \to 0$ here). What differs is the wave amplitude itself, since $B_s \neq B_L$.

Using (4.10), the criterion becomes

$$-2C\eta^{-1}\theta^3 > 1. \quad (4.17)$$

Hence if $C/\eta > 0$ the positive solutions of Fig. 7 are stable, while the negative solution is stable if $C/\eta < 0$, in which case there is at least one steady, stable solution for all $\sigma\eta^{-1/3}$. In fact, since on the lower curve $\theta = -2^{2/3}$ at $q = q_c$, the lower solution is stable in $\sigma\eta^{-1/3} > q_c$ if $C/\eta < \frac{1}{8}$ and there is then one stable steady solution for all $\sigma\eta^{-1/3}$. We shall see that this criterion is satisfied and, in fact, $C/\eta < 0$ in most cases of interest.

If $0 > C/\eta > -1$, the whole of the linear "high-index" curve—the lower half of the positive curve—is stable and there are in $\sigma\eta^{-1/3} < q_c$ at least two stable steady solutions, as first noted by Charney and DeVore (1979). Indeed if $|C/\eta|$ is much smaller than unity, parts of the third, upper curve also become stable. However, this solution becomes unstable at sufficiently large negative $\sigma$.

If $C/\eta < -1$ the whole of the upper curve and parts of the "high-index" curve become unstable although the latter solution is always stable at large negative $\sigma$.

Typical values of $C/\eta$ as a function of $\mathrm{F}U/\beta$ and $\kappa^2$ are shown in Fig. 8 for the first wave mode with $m = 1$ and $\mathrm{F} = \pi^2$ (results for the second mode and with other parameters are similar). $C/\eta < -1/8$ everywhere except in a narrow band $28 < \kappa^2 < 34$, where $C/\eta$ may be positive. In this region, the negative steady solution may be unstable and, therefore, there may be a range of $\sigma$ for which there is no stable steady solution. However, this regime lies at wavelengths substantially smaller than the Rossby deformation radius and is unlikely to be of practical interest—certainly not for atmospheric planetary waves. In the region of interest, then, our results accord with those of previous studies—for $\sigma > q_c\eta^{1/3}$, there is one stable solution while there are two (and perhaps three) for $\sigma < q_c\eta^{1/3}$, only one of which resembles the linear solution.

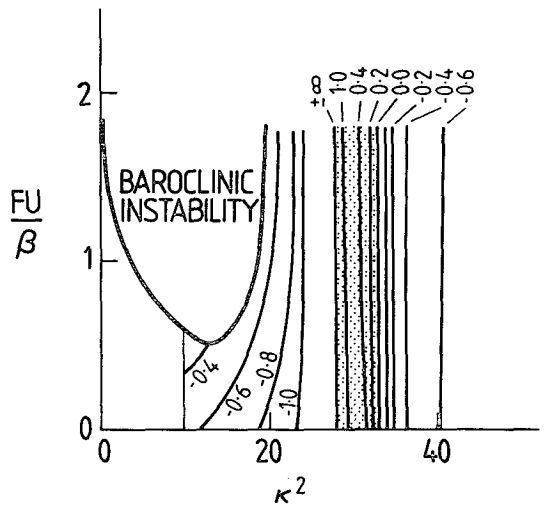


FIG. 8. The ratio $C/\eta$ for the first wave mode as a function of $U$ and $\kappa^2$ for $m = 1$, $F = \pi^2$. Regions where $C/\eta > -\frac{1}{8}$ are shaded. (Note that $\kappa^2 \geq \pi^2$ for $m = 1$). Heavy curve: baroclinic instability threshold.

### c. *Transient solutions*

The decay of the periodic inviscid solutions and their relationship with the steady viscous solutions are illustrated by explicit numerical integration of (4.4) and (4.5) with the initial condition $\chi_n(0) = 0$. The series in (4.5) was truncated at $n = 5$, which tests showed to be more than adequate for convergence. The data used for these runs, together with the derived coefficients $a_n$, $C$ and $\eta$ are shown in Table 1; various values of $\sigma$ and $r$ were used.

For positive $\sigma$, $\sigma\eta^{-1/3} > 0$ and there is only one stable steady solution. The inviscid evolution $r = 0$ is shown in Fig. 9a for $\sigma = 1$, $C/\sigma^3 = -0.053$. In agreement with Fig. 5, the inviscid evolution is a closed orbit around the linear solution $B_L$. Viscous adjustment to the steady state is shown in Fig. 9b, with $r = 0.03$; the solution spirals into $B_s$ as the free-wave mode (excited by the initial conditions) decays.

At large negative $\sigma$ there are two stable solutions. However, for $|\sigma\eta^{-1/3}| \gg 1.89$ all cases studied with initial conditions were captured into the quasi-linear "high-index" mode. This is illustrated in Fig. 10, with $\sigma = -1.5$ mg ($\sigma\eta^{-1/3} = -2.68$). Then $C/\sigma^3 = 0.016$; the inviscid behavior (Fig. 10a) in all cases shown is the form of an inner orbit around $B_L$. This is to be expected for this small value of $C/\sigma^3$, although one might anticipate bifurcation at sufficiently large

TABLE 1. Data used for the numerical integration of Eqs. (4.4) and (4.5).

| Basic data | | Derived coefficients | |
|---|---|---|---|
| $m$ | 1 | $a_1$ | 1.073 |
| $\kappa^2$ | 15 | $a_2$ | 0.527 |
| F | $\pi^2$ | $a_3$ | −0.038 |
| $\beta$ | 30 | $a_4$ | 1.298 |
| $\Lambda_0$ | 1 | $C$ | −0.053 |
| | | $\eta$ | 0.177 |

$|B(0)|$. Fig. 10b shows the viscous behavior, with $r = 0.03$. In all cases, $B$ spirals into the "high-index" solution $B_s$ (which is very close to $B_L$).

As $\sigma\eta^{-1/3}$ approaches $-1.89$, the amplitude of the nonlinear solution decreases and nonlinear effects become more important. Concomitantly the attractor basin of the quasi-linear solution recedes, a process which, as will be seen in the next example, is related to the inviscid behavior discussed in Section 3. Examples with $\sigma = -1.12$ ($\sigma\eta^{-1/3} = -2.0$, $C/\sigma^3 = 0.037$) are presented in Fig. 11. The inviscid trajectories are such that, from $B(0) = (0, 0)$, $B$ orbits the linear solution at $B_L = (0.89, 0)$ but, starting from $B(0) = (-2, 0)$, the outer nonlinear track is followed. The damped case (Fig. 11b) shows a similar duality of behavior. There are stable steady solutions at $B_s = 1.12$ and $-2.88$ as $r \to 0$. It is seen that with $B(0) = (0, 0)$, $B$ spirals into the quasi-linear solution while for $B(0) = (-2, 0)$, the wave evolves to the nonlinear, "low-index" solution as $\tau \to \infty$. (Note that because $r$ is finite, the steady solutions in Fig. 11b are located slightly off the real axis.) During the first few spindown times ($\tau \lesssim r^{-1}$) the trajectories are close to those of the inviscid problem and it is clear that this early evolution plays an important role in directing $B$ into the attractor basin of one or the other of the steady damped solutions. Finally, note that the third steady solution at $B_s = 1.78$ is also stable according to (4.16), but it proved difficult to find initial conditions that would lead to it. Experience with several such cases gave the impression that this second "low-index" solution is destabilized by finite $r$.

It should not be deduced from the above example that there is necessarily a one-to-one correspondence between the inviscid bifurcation and mode selection in the damped problem. We now consider $\sigma = -0.9$ ($C/\sigma^3 = 0.073$, $\sigma\eta^{-1/3} = -1.61$). Inviscid cases with $B(0) = (0, 0)$ and $(-1, 0)$ (Fig. 12a) show the same dual behavior as in the previous example. There is now, however, only one damped steady state (at $B_s = -2.96$ as $r \to 0$)—the quasi-linear solution does not exist here. With $r = 0.03$ (Fig. 12b) evolution from $B(0) = (-1, 0)$ is again as in Fig. 11, $B$ spiraling into the $B_s$. From $B(0) = 0$, however, $B$ follows a peculiar trajectory. Initially it spirals from the inviscid track as if into a nonexistent quasi-linear solution. After some time ($\tau \approx 200$ or about six spindown times) this behavior changes as $B$ moves outward again and into an "outer" track before spiraling into $B_s$. Similar behavior has previously been noted by Hart (1979).

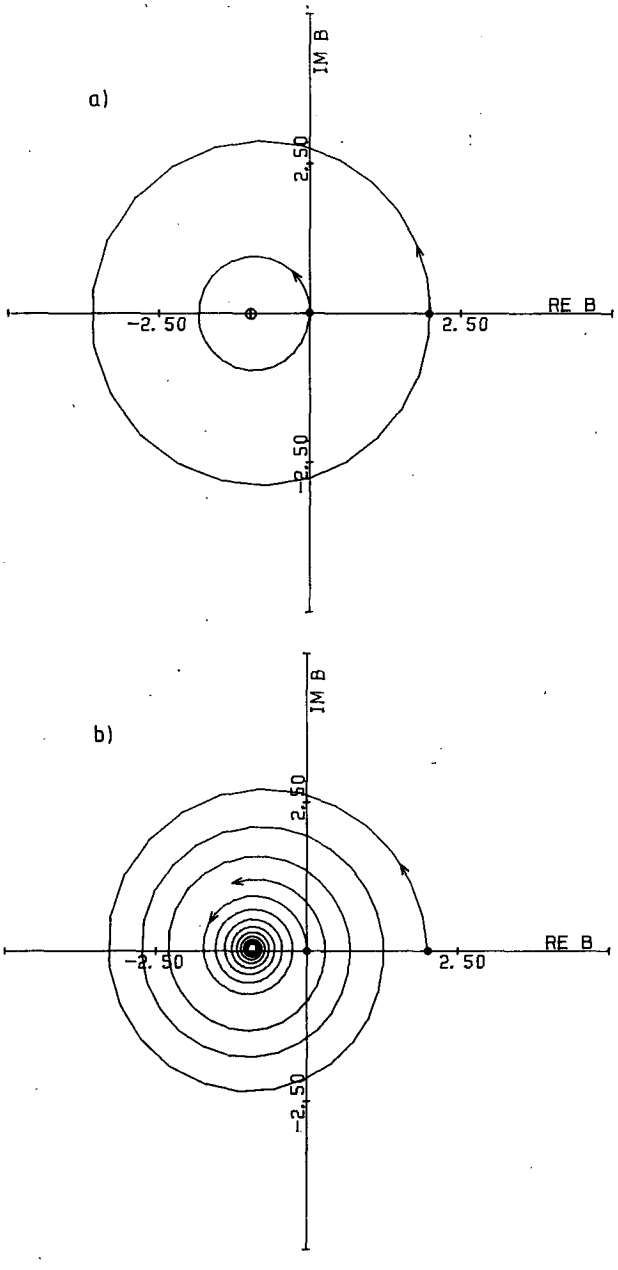


FIG. 9. (a) Undamped ($\tau = 0$) and (b) damped ($\tau > 0$) evolution at positive $\sigma$ ($C = -0.053$, $\eta = 0.177$). $\sigma = 1$. Trajectories are plotted every $\Delta\tau = 0.5$. Arrows denote direction of evolution, closed circles denote initial value of $B$. (a) $r = 0$, $\oplus$ denotes linear solution $B_L$. (b) $r = 0.03$.

Fig. 13 shows trajectories for the same parameters as in Fig. 12, but initial conditions such that $B(0) \approx B_L$. This case may be regarded as an example of the transition that would occur if $\sigma$ were suddenly reduced from a value such that $\sigma\eta^{-1/3} < -1.89$ to one with $\sigma\eta^{-1/3} > -1.89$. The initial conditions thus approximate the quasi-linear solution in the original state; this solution no longer exists in the new state. Note, however, that the linear solution $B_L$ is stable

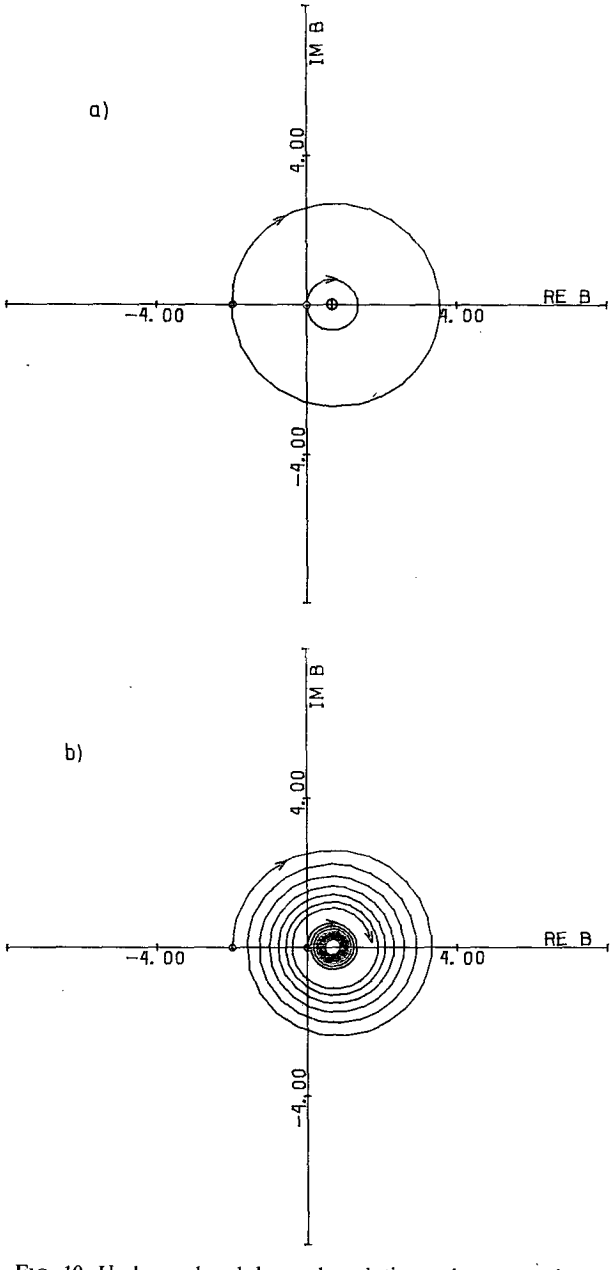


FIG. 10. Undamped and damped evolution at large negative $\sigma$. As in Fig. 9 except $\sigma = -1.5$.

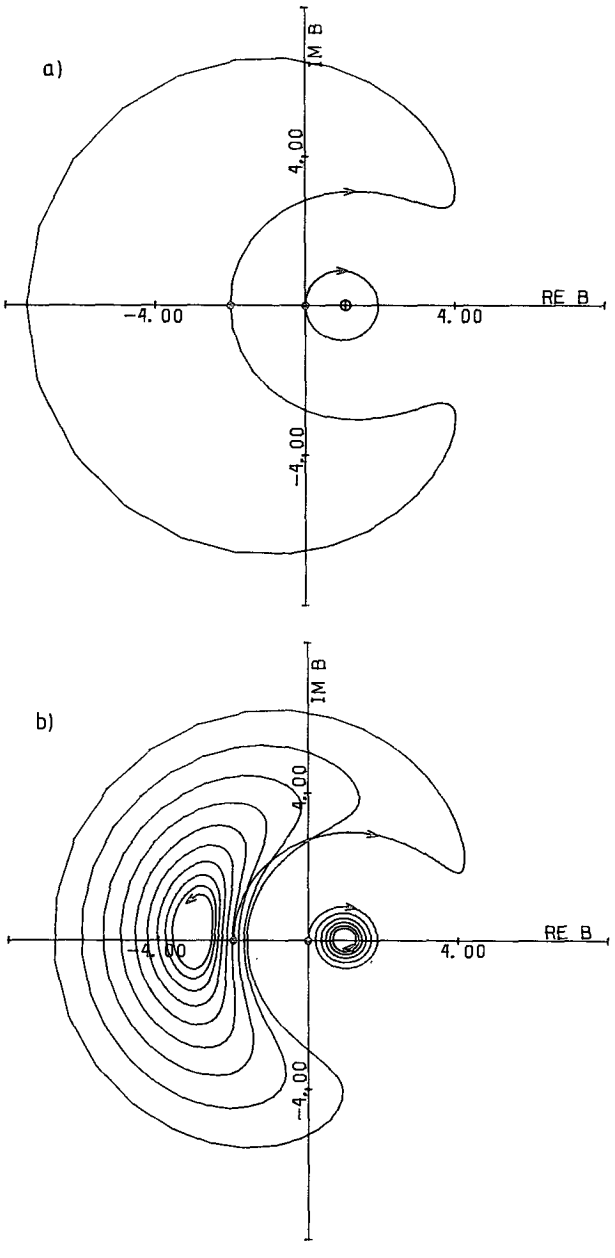


FIG. 11. Undamped and damped evolution at moderate negative $\sigma$. As in Fig. 9 except $\sigma = -1.12$.

in an inviscid sense ($C/\sigma^3 < \frac{1}{2}$) and therefore it is expected that $B$ will remain in the vicinity of $B_L$ for a time of order $r^{-1}$ before evolving toward $B_s$. This is indeed what happens, as shown in Fig. 13. With $r = 0.03$ (Fig. 13a), $B$ remains close to $B_L$ until $\tau \approx 125$ after which it evolves more rapidly into an "outer" track and spirals into $B_s$. Evolution away from $B_L$ is more rapid for larger $r$; Fig. 13 also shows the trajectory for $r = 0.1$. Thus, adjustment away from $B_L$ takes several spindown times.

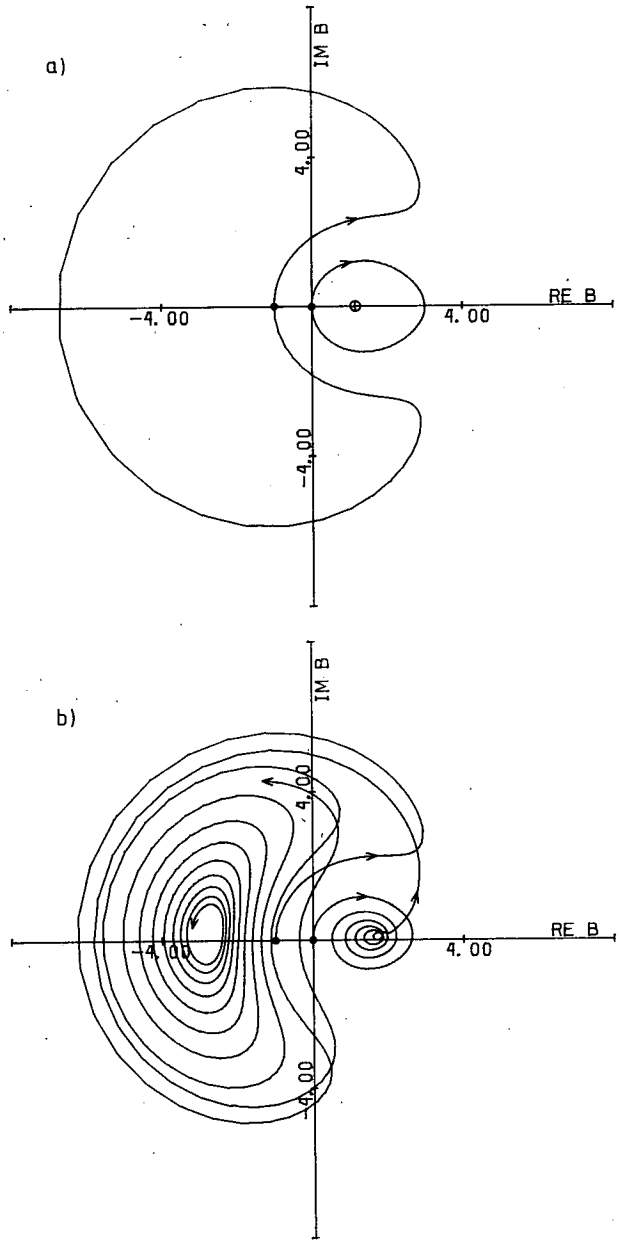


FIG. 12. Undamped and damped evolution at small negative $\sigma$. As in Fig. 9 except $\sigma = -0.9$.

As $|\sigma|$ is reduced further so that $C/\sigma^3 > \frac{1}{2}$, however, the linear solution becomes unstable on the inviscid time scale and transition to the steady solution becomes more rapid. This is illustrated in Fig. 14 with $\sigma = -0.4$ ($\sigma\eta^{-1/3} = -0.71$, $C/\sigma^3 = 0.83$). In the inviscid problem, the trajectory, as in Fig. 3, is an "outer" track of period $\tau \approx 25$. The viscous evolution with $r = 0.03$ is similar; the orbital period is reduced to about 15 and $B$ spirals into $B_s$. In this regime, then, evolution away from the nonexistent quasi-linear "solution" is much more rapid than when $B_L$ is stable in the inviscid problem. The inviscid behavior discussed in Section 3 is in fact valid (to a good approximation) for several spindown times and may be more relevant than the viscous steady states in problems where this type of analysis has limited validity in time (because, for example, of non-steadiness of the background mean state or of the forcing mechanism).

## 5. Conclusions

Several potentially important features emerge in or are clarified by this analysis. The evolution equation obtained is a cubic in wave amplitude, a common result in this kind of problem [for example, the anharmonic oscillator (see Landau and Lifshitz, 1960, §29)] and in agreement with the result of Charney and DeVore (1979). This is a result of the truncation which limits the number of degrees of freedom of the model. In Charney and DeVore's study, the truncation was made *a priori* as a simplifying device, whereas in this study it is the wave amplitude which is assumed small *a priori*; the truncation to a simple wave, mean-flow interaction problem then follows as a natural and self-consistent consequence. The analysis has been restricted to near-resonant forcing simply as a matter of expediency; far from resonance, no nonlinear effects are significant.

In the undamped problem, solution behavior is in general the result of interaction of the mean flow with the forced wave and a free traveling wave whose phase velocity and amplitude are modified by the interaction. Where the feedback is weak or negative the complex wave amplitude performs a simple orbit (in phase space) of the linear solution. If the feedback is positive and sufficiently strong, the traveling wave may become temporarily locked into

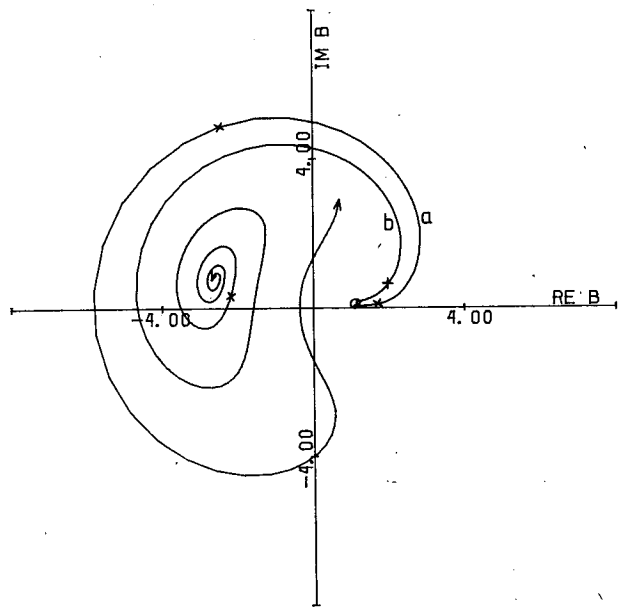


FIG. 13. Damped evolution away from the linear solution $B_L$ when $B_L$ is stable under inviscid dynamics. $\sigma = -0.9$, $B(0) = (1.1, 0)$. Trajectory plotted every $\Delta\tau = 0.2$. (a) $r = 0.03$, $\times$ denotes location of $B$ at $\tau = 125, 150$. (b) $r = 0.1$, $\times$ denotes location of $B$ at $\tau = 50, 75$.

a nonlinear resonance, during which time its amplitude increases markedly. The complex wave amplitude then performs a periodic "outer" orbit which does not enclose the linear solution. This behavior manifests itself most dramatically in cases of strong positive feedback when the linear solution becomes unstable as a result of growth of an initially weak traveling wave.

In the presence of damping, one or three steady states are possible, one, two or three of which may be stable. Even in the limit of vanishing viscosity, these steady states do not all correspond with the inviscid solution; far from resonance, however, one of the solutions does so. Charney and DeVore (1979) identified the other, nonlinear, solutions as "low-index" states associated with nonlinear resonance (see also Trevisan and Buzzi, 1980) and remarked on their similarity to atmospheric blocking patterns. Egger (1978) found blocking to occur in a series of numerical experiments, apparently arising from a mechanism similar to that discussed here. In the present work, attention has been drawn to the transient behavior as the forced wave adjusts toward steady state. On time scales less than several spindown times the wave evolution is governed essentially by inviscid dynamics. On longer time scales the complex wave amplitude spirals (in phase space) into one of the stable steady solutions. Where more than one such stable solution exists the selection of the final state is largely determined by the inviscid trajectory adopted during the early stages of evolution.

Previous authors on this topic have noted the likely relevance of these properties to our understanding of atmospheric planetary waves. In most cases emphasis has been directed at tropospheric blocking, although Davey (1980) has noted possible oceanic applications. Perhaps the most spectacular manifestation of planetary wave-mean flow interaction is the sudden warming phenomenon of the winter stratosphere. In this region the damping time scale (via radiation) is typically 10 days, so that over time scales less than a month or so it is unlikely that damped steady states can be established and undamped solutions of the type found here may be relevant to the problem. Such a restrictive model as this cannot be applied directly, of course, but it will be shown in a following paper (Plumb, 1981) that the corresponding continuous model is governed by the same evolution equation (3.4) and that the solutions found here provide a simple explanation of the bifurcation and feedback phenomena found in highly truncated models of stratospheric warmings.

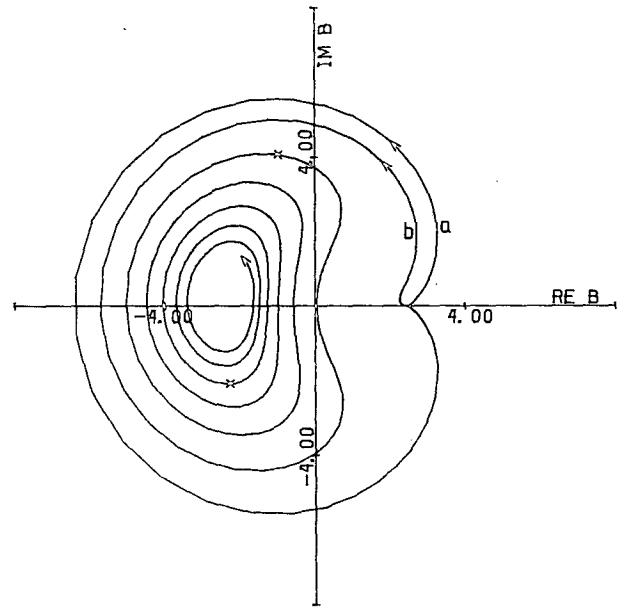


FIG. 14. Damped evolution away from the linear solution $B_L$ when $B_L$ is unstable under inviscid dynamics. $\sigma = -0.4$, $B(0) = (2.5, 0.01)$. Trajectory plotted every $\Delta\tau = 0.2$. Arrow shows direction of evolution. (a) $r = 0$ and (b) $r = 0.03$ (trajectory terminates after $\tau = 75$). × denotes location of $B$ at $\tau = 25$, 50.

## REFERENCES

Charney, J. G., and J. G. DeVore, 1979: Multiple flow equilibria in the atmosphere and blocking. *J. Atmos. Sci.*, **36**, 1205–1216.

——, and D. M. Straus, 1980: Form-drag instability, multiple equilibria and propagating planetary waves in baroclinic, orographically forced, planetary wave systems. *J. Atmos. Sci.*, **37**, 1157–1176.

Davey, M. K., 1980: A quasi-linear theory for rotating flow over topography. Part 1. Steady $\beta$-plane channel. *J. Fluid Mech.*, **99**, 267–292.

Egger, J., 1978: Dynamics of blocking highs. *J. Atmos. Sci.*, **35**, 1788–1801.

Fischer, G., 1980: The effect of a planetary scale mountain on a barotropic flow treated in a simple low-order system. *Beitr. Phys. Atmos.*, **53**, 295–309.

Hart, J. E., 1979: Barotropic quasi-geostrophic flow over anisotropic mountains. *J. Atmos. Sci.*, **36**, 1736–1746.

Landau, L. D., and E. M. Lifshitz, 1960: *Mechanics; Course of Theoretical Physics*, Vol. 1. Pergamon Press, 165 pp.

McEwan, A. D., R. O. R. Y. Thompson and R. A. Plumb, 1980: Mean flow driven by weak eddies in rotating systems. *J. Fluid Mech.*, **99**, 655–672.

Paegle, J. N., 1979: The effect of topography on a Rossby wave. *J. Atmos. Sci.*, **36**, 2267–2271.

Pedlosky, J., 1970: Finite-amplitude baroclinic waves. *J. Atmos. Sci.*, **27**, 15–30.

——, 1971: Finite-amplitude baroclinic waves with small dissipation. *J. Atmos. Sci.*, **28**, 587–597.

Plumb, R. A., 1979: Forced waves in a baroclinic shear flow. Part 1: Undamped evolution near the baroclinic instability threshold. *J. Atmos. Sci.*, **36**, 205–216.

——, 1981: Nonlinear planetary waves in a continuous baroclinic shear: Application to stratospheric warmings. Submitted to *J. Atmos. Sci.*

Romea, R. D., 1977: The effects of friction and $\beta$ on finite-amplitude baroclinic waves. *J. Atmos. Sci.*, **34**, 1689–1695.

Smith, R. K., 1977: On a theory of amplitude vacillation in baroclinic waves. *J. Fluid Mech.*, **79**, 289–306.

Trevisan, A., and A. Buzzi, 1980: Stationary response of barotropic weakly nonlinear Rossby waves to quasi-resonant orographic forcing. *J. Atmos. Sci.*, **37**, 947–957.